LUND UNIVERSITY

Dopant Engineering of Inter-Subband Linewidth and Lineshape in Multiwell Heterostructures

Ndebeka-Bandou, Camille; Wacker, Andreas; Carosella, Francesca; Ferreira, Robson; Bastard, Gerald

Link to publication

Dopant engineering of inter-subband linewidth and lineshape in multi-well heterostructures

C. Ndebeka-Bandou[1], A. Wacker[2], F. Carosella[1], R. Ferreira[1], G. Bastard[1,3]

[1] *Laboratoire Pierre Aigrain, Ecole Normale Supérieure, CNRS (UMR 8551), Université P. et M. Curie, Université Paris Diderot, 24 rue Lhomond F-75005 Paris, France*
[2] *Mathematical Physics, Lund University, Box 118, S-22100 Lund, Sweden*
[3] *Technical University Vienna, Photonics Institute, Gusshausstrasse 27, A-1040 Vienna, Austria*

We show by numerical diagonalization of the electronic Hamiltonian including screened Coulombic impurities that the inter-subband absorption lineshape and linewidth in heterostructures can be controlled by a suitable location of the dopants. We also point out that the usual optical conductivity calculations that employ the self consistent Born approximation often lead to incorrect lineshapes although the trends for the linewidths versus the dopant location are the same as found in the present numerical approach.

It is well established that there exist many possibilities to taylor the widths and barrier heights of multi-well heterostructures in order to produce a given set of energy levels. The ultimate accomplishment of this bandgap engineering is probably the Quantum Cascade Laser[1] where lasing between subbands with a prescribed energy difference has been realized thanks to a very precise control of the widths of hundreds of layers. The inter-subband transition lineshape of an ideal structure is a delta function peaked at the subband energy difference, if non parabolicity is neglected.[2] Actual samples display an inter-subband absorption linewidth that is affected by inelastic and elastic scatterers, which essentially perturb the in-plane motion of electrons.[3–6] One of them, the scattering at the Coulomb potential of ionized impurities, is unavoidable due to the requirement of supplying carriers. They are known to be of relevance and the corresponding scattering rate surpasses, e.g., the electron-electron scattering.[7] In this letter we will show that there exists room for a dopant engineering that allows a manipulation of the absorption and emission lineshapes in typical Quantum Cascade Laser (QCL) structures. We will show that a suitable placement of donor atoms results in a narrowing of the inter-subband lineshape, and that one may create at will inter-subband absorption lines that comprise one or two peaks (the latter effect has already been observed[8]). Moreover, we will show that despite the in-plane disorder due to coulombic impurities and interface defects (witnessed by the width of the spectral function) there exists quasi-selection rules for inter-subband absorption; in other words that the width of the inter-subband absorption line can be very small while the intra-subband scattering is very strong.

The structure we are going to use as representative example is a $GaAs/Ga_{0.75}Al_{0.25}As$ Double

Quantum Well (DQW) with $L_1 = 9$ nm, $L_2 = 3$ nm and an intermediate barrier width of $h = 2$ nm. The conduction band offset is 217.5 meV. There are three bound states in this structure labelled E_n, $n = 1, 2, 3$. In the following, we study the optical transitions between E_1 and E_2 subbands with an unperturbed energy $E_2 - E_1 = 73.8$ meV. We shall consider a diluted concentration of donor impurities $n_{imp} = 2.17 \times 10^{10}$ cm^{-2}. This corresponds to 8 impurities randomly placed on a $S = 200$ nm $\times$ 200 nm (x, y) plane located at $z = z_l$. These impurities are screened by mobile electrons and we use the three dimensional Debye Hückel screening: each screened ionized donors located at $\vec{r}_p = (\vec{\rho}_p, z_l)$ creates a Yukawa potential

$$V_{SC}(\vec{r} - \vec{r}_p) = -\frac{e^2}{4\pi\varepsilon_0\varepsilon_r|\vec{r} - \vec{r}_p|}\exp\left(-\frac{|\vec{r} - \vec{r}_p|}{\lambda}\right) \tag{1}$$

where $\lambda = \sqrt{\frac{\varepsilon_0\varepsilon_r k_B T}{e^2 n_{3D}}}$ is the Debye screening length with ε_r the static dielectric constant and n_{3D} the equivalent three dimensional electronic concentration (see Ref.[9] for a discussion).

The numerical calculations have been performed by diagonalizing the complete Hamiltonian

$$H = \frac{p^2}{2m^*} + V_b(z) + V_{imp}(\vec{r}) \tag{2}$$

$$V_{imp}(\vec{r}) = \sum_p V_{sc}(\vec{r} - \vec{r}_p) \tag{3}$$

including coulombic impurities on a basis of plane waves that are periodic in the 200 nm $\times$ 200 nm box. By expanding on the two subbands E_1 and E_2:

$$\Psi_\nu(\vec{\rho}, z) = \sum_n \varphi_{\nu,n}(\vec{\rho})\chi_n(z) \tag{4}$$

$$-\frac{\hbar^2}{2m^*}\nabla^2\varphi_{\nu,n} + \sum_{n'} V_{imp}^{n,n'}\varphi_{\nu,n'} = (\varepsilon_\nu - E_n)\varphi_{\nu,n} \tag{5}$$

$$V_{imp}^{n,n'} = \int dz\chi_n(z)\chi_{n'}(z)V_{imp}(\vec{r}) \tag{6}$$

where $n = 1, 2$ and ν labels the eigenstates of the complete Hamiltonian for a given realization of disorder. $\varphi(\vec{\rho})$ is the in-plane envelope function. With the numerically calculated eigenstates and eigenenergies, we will compute the absorption coefficient of an electromagnetic wave that propagates in the layer plane with its polarization parallel to z growth axis:[10, 11]

$$\alpha(\omega) = \frac{2\pi}{m^{*2}\omega\varepsilon_0 cnL_z S}\sum_{\nu,\mu}(f_\nu - f_\mu)|\langle\Psi_\nu|p_z|\Psi_\mu\rangle|^2 \times \delta(\varepsilon_\mu - \varepsilon_\nu - \hbar\omega) \tag{7}$$

where n_r is the refractive index, L_z is the effective thickness of the waveguide in relation to the active region considered – for QCLs filling the entire waveguide this is one period, and we use $L_z = 19.6$ nm here. f_ν is the occupation of the state Ψ_ν which we take as a Fermi-Dirac function using $T = 100$ K throughout this paper. For our numerical study, we consider different statistical realizations of disorder and the results to be presented below are the average over 30 such trials.

The numerical solutions are exact but may be cumbersome to obtain. There however exist many ways to compute approximately the effects of disorder on the eigenstates as well as the optical con-
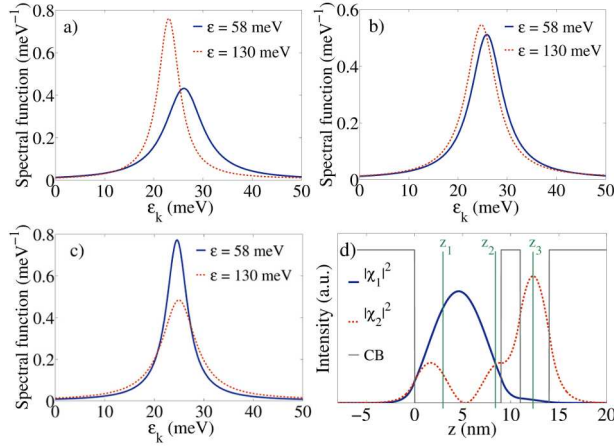
Fig. 1. Spectral functions versus the kinetic energy for two energies $\varepsilon = 58$ meV and 130 meV and for three dopant locations: $z_l = 3$ nm (panel a), $z_l = 8.45$ nm (panel b), $z_l = 12.3$ nm (panel c). Panel d shows the conduction band profile of the DQW and the squared modulus of the χ_1 and χ_2 envelope wavefunctions. The vertical green solid line represent the impurity plane positions: $z_1 = 3$ nm, $z_2 = 8.45$ nm and $z_3 = 12.3$ nm.

ductivity perturbatively. Unuma *et al.*[6] used Ando's approach[3,4] based on a density matrix treatment of the conductivity to evaluate the absorption coefficient. As shown in Ref.[12] a Non Equilibrium Green's Function (NEGF) formalism within the self-consistent Born approximation provides essentially similar results, but allows to treat QCLs self-consistently under operating conditions, for details see Ref.[13] In this formalism broadening of the unperturbed states of subband n with in-plane motion k is expressed by the spectral functions[14]

$$A_n(\varepsilon, k) = \frac{-2\Im\{\Sigma_n(\varepsilon, k)\}}{\left(\varepsilon - E_n - \frac{\hbar^2 k^2}{2m^*} - \Re\{\Sigma_n(\varepsilon, k)\}\right)^2 + \Im\{\Sigma_n(\varepsilon, k)\}^2} \tag{8}$$

where $\Sigma_n(\varepsilon, k)$ is the retarded electron self-energy. Evaluating the dynamical conductivity with all self-energy corrections, provides a linewidth, which is typically of the order of $-2\Im\{\Sigma\}$ for the involved states, but can also show compensation effects.[12]

Since we consider a dilute concentration of impurities, except in the vicinity of these impurities there is $|\vec{\rho} - \vec{\rho}_p| \gg |z - z_l|$ and the matrix element of the single impurity Coulomb potential reduces to

$$V_{SC}^{n,n'}(|\vec{\rho} - \vec{\rho}_p|) \approx -\frac{e^2}{4\pi\varepsilon_0\varepsilon_r|\vec{\rho} - \vec{\rho}_p|} \times \exp\left(-\frac{|\vec{\rho} - \vec{\rho}_p|}{\lambda}\right)\delta_{nn'} \tag{9}$$

On the other hand, very close from an impurity center there is

$$V_{SC}^{n,n'}(|\vec{\rho} - \vec{\rho}_p|) \approx -\frac{e^2}{4\pi\varepsilon_0\varepsilon_r}\chi_n(z_l)\chi_{n'}(z_l)\ln(|\vec{\rho} - \vec{\rho}_p|) \tag{10}$$

Hence, we see that the effective potential close to the impurity has a weaker divergence than a coulombic law and that the strength of the short range potential depends explicitly on the location of the dopant plane. It can immediately be anticipated that the latter feature is at the heart of the dopant engineering.

In fact, Figs. 1a,b,c show the spectral functions $A_n(\varepsilon, k)$ plotted versus $\frac{\hbar^2 k^2}{2m^*}$ for the subband $n = 1$ at $\varepsilon = 58$ meV and for $n = 2$ at $\varepsilon = 130$ meV at three dopant positions: $z_l = 3$ nm, 8.45 nm and 12.3 nm, respectively. The two chosen energies correspond in the unperturbed DQW to E_1 and E_2 subband states with roughly the same kinetic energy for the in-plane motion. At $z_l = 3$ nm, a position where the subband 1 is more affected by the Coulomb potential than the subband 2 ($|\chi_1(z_l)|^2 > |\chi_2(z_l)|^2$), the width of the spectral function for subband 1 is wider than the one for subband 2. At the same time, the real part of the self-energy is more negative for state 1. Conversely, at $z_l = 12.3$ nm which corresponds to the maximum of $|\chi_2(z)|^2$, state 2 is more affected by the Coulomb scattering, and thus has a larger width and a more negative real part of the self-energy. Finally, at $z_l = 8.45$ nm, the spectral functions are very simliar, as the two subbands are affected in about the same manner since $|\chi_1(z_l)|^2 \approx |\chi_2(z_l)|^2$. In all cases the width of the spectral functions is of the order of 10 meV, and consequently, a corresponding linewidth for the absorption spectrum, would be expected.

We show in Fig. 2a the absorption spectra for the three dopant positions used in Fig. 1 as calculated by numerical diagonalization. At first we notice, that the absorption spectra are shifted from the bare transition energy of 73.8 meV corresponding to the relative shifts of the spectral functions. Secondly, the absorption spectra for $z_l = 3$ nm and $z_l = 12.3$ nm display two peaks. At third, there is only a single peak for $z_l = 8.45$ nm, whose width is more than an order of magnitude smaller than the width of the spectral functions. These features can be well understood by considering the density of states (DOS) and the dipole matrix elements as shown in Fig. 3. For the low dopings considered, the density of states exhibits a set of impurity related states at the bottom of each subband, whose seperation from the main band increases with the magnitude of the respective scattering matrix elements. At $z_l = 3$ nm, the set of impurity states below the first subband is more pronounced, and absorption to the bottom of the second subband provides the peak around 78.5 meV (Fig. 2a). The second peak around 74.3 meV is due to transtions between the continuum of both subbands. Fig. 3a shows, that the dipole matrix element essentially only connects states with a constant energy difference, which results in the narrow line width. Conversely, for $z_l = 12.3$ nm, the set of impurity states below the second subband is more pronounced, which reverts the scenario. The situation for $z_l = 8.45$ nm is peculiar since the scattering strength is almost identical for both subbands. Thus the transitions between the set of impurity states of both subbands have the same energy as the transistions between conventional subband states and there is only one peak. Fig. 3b shows that the matrix element for the optical transions is very selective and thus the linewidth is very narrow. It is interesting to point out that inter-subband absorption lineshapes comprising two peaks have already been observed in doped superlattices and doped quantum well structures.[8,15] Only a numerical modeling of the superlattice absorption was capable to account for the double peak feature. In addition, varying the temperature affects the weight of the two absorption peaks as discussed by Stehr *et al.* for very dilute impurities.[16] Note that in the present model we neglected the depolarization effects because of the smallness of the carrier concentration. As a matter of fact, by using Unuma's *et al.* formula (Eq. 14 in Ref.[6]), and assuming an oscillator strength of 1
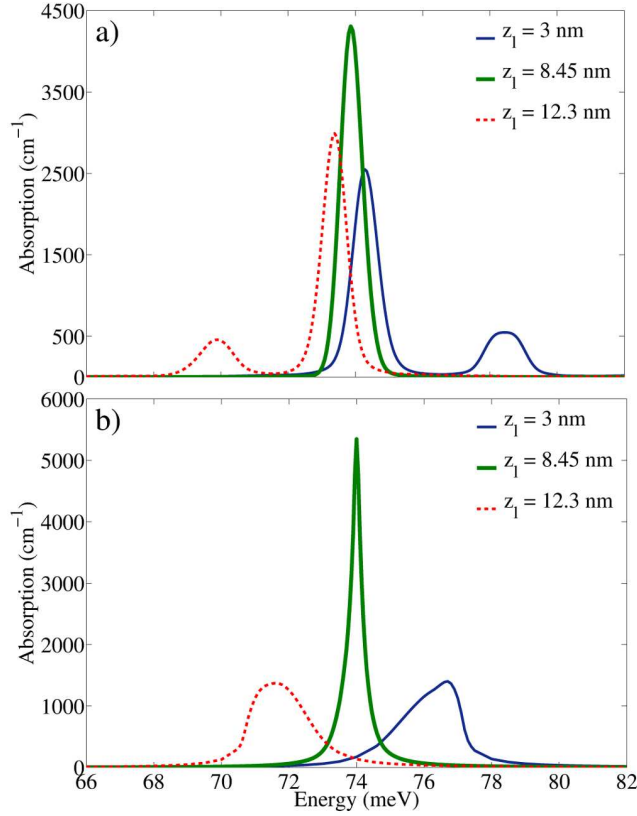
Fig. 2. Absorption spectrum for the E_2-E_1 transition calculated by numerical diagonalization (Panel a) and by using NEGF formalism (Panel b) for three dopant locations: $z_l = 3$ nm (blue dashed-dotted line), $z_l = 8.45$ nm (green solid line) and $z_l = 12.3$ nm (red dotted line). $n_{\mathrm{imp}} = 2.17 \times 10^{10}$ cm^{-2}. $T = 100$ K.

and an effective thickness of the 2D electron gas equal to $L_1 + h + L_2$, we find a plasma energy of 5 meV and thus a depolarization shift of 0.17 meV, which is negligible compared to the energy of the impurity related localized states.

Most perturbative approaches, such as the self-consistent Born approximation, only take into account quadratic terms of the scattering potential. These are not able to reproduce impurity related localized states, which are multiple scattering events.[17] Thus, they result in single peak spectra, as shown in Fig. 2b for the NEGF approach. Nevertheless, the full self-consistent treatment[12] allows for a good description of the narrow lines and the trends for the shift from the bare resonance are correctly reproduced.

Both the exact diagonalization as well as the NEGF method predict very narrow inter-subband absorption lineshapes when the wavefunction amplitudes for the z motion are about the same, at the doping plane $z = z_l$, for the initial and final subbands. In fact, while the electrons undergo scatterings on coulombic impurities, there seems to exist a quasi selection rule for the inter-subband absorption (Fig. 3). The contour plot of the dipole matrix element $|\langle \nu | p_z | \mu \rangle|^2$ confirms this feature. Namely, there is an extremely narrow energy range around the diagonal $|\varepsilon_\mu - \varepsilon_\nu| \approx E_2 - E_1$ where the states have a
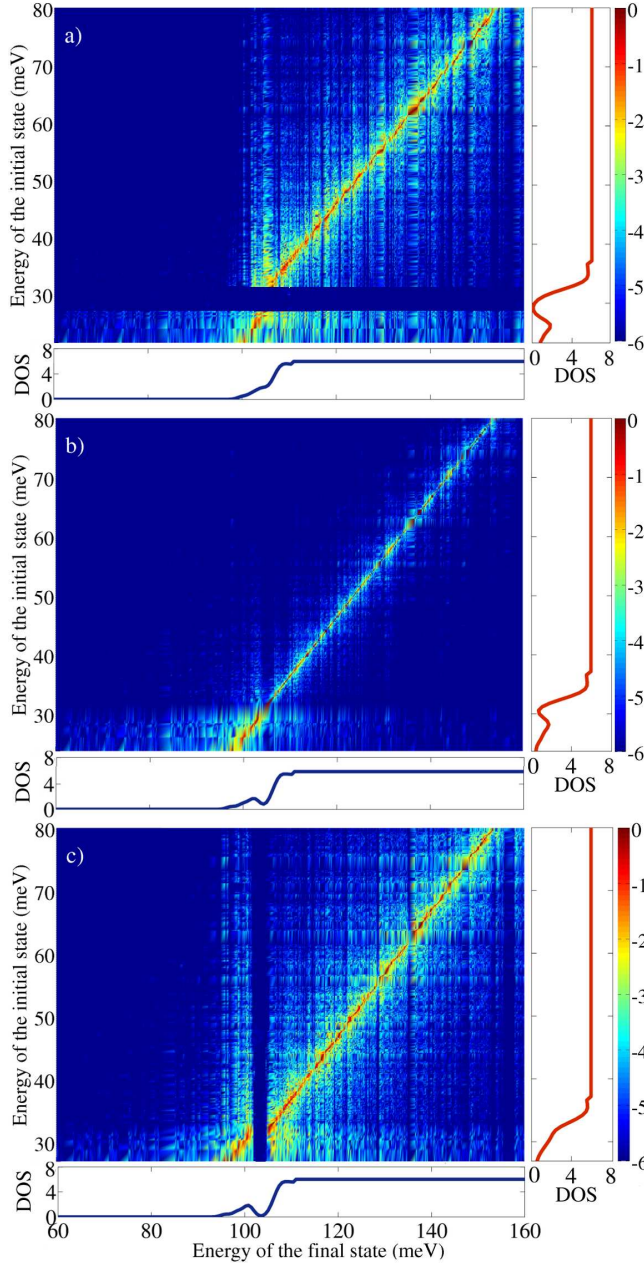
Fig. 3. Contour plot of the decimal logarithm for the optical matrix element $|\langle \nu|p_z|\mu\rangle|^2$ as a function of the energies ε_μ and ε_ν for the optical transitions studied in Fig. 2a. Panels a),b) and c) correspond to $z_l = 3$ nm, 8.45 nm, and 12.3 nm, respectively. On the axes, the DOS for the initial states (red solid line) and final states (blue solid line) are plotted in units of meV^{-1}. $E_2 = 107.46$ meV. The blue stripes around $\varepsilon_\nu \approx 30$ meV (in a) and $\varepsilon_\mu \approx 105$ meV (in c) indicate the vanishing density of states.

significant dipole matrix element. Note that there exists a deviation at low energy for $z_l = 3$ nm and 12.3 nm. It corresponds to the optical transitions between the bound states attached to the E_1 subband and the quasi bound states below the E_2 subband. These effects are not taken into account by standard perturbative approaches, such as the Born approximation.

In conclusion, we have shown that a "dopant engineering" in heterostructures leads to several interesting features. Firstly, our numerical approach confirms that one might get very narrow inter-subband absorption lines in spite of a very strong broadening of the subband states, which can be seen both from our exact study and the NEGF approach. However, one has to bear in mind, that the Born approximation does not reproduce correctly the impurity related localized states and thus, it cannot correctly reproduce the double peak scenario, which is found, if one state is more affected by the impurities than the other. Unless one engineers the doping in a way that ensures nearly equal wavefunction amplitudes on the dopant plane, the inter-subband absorption usually displays two peaks. This is the same for the inter-subband emission (not shown). The existence of two peaks modifies the absorption profile significantly and thus is important for a realistic description of low doped devices.

Acknowledgement

References

1) J. Faist, F. Capasso, D. L. Sivco, C. Sirtori, A. L. Hutchinson and A. Y. Cho, Science **264** (1994) 553

2) C. Sirtori, F. Capasso, J. Faist and S. Scandolo, Phys. Rev. B **50** (1994) 8663

3) T. Ando, A. B. Fowler and F. Stern, Rev. Mod. Phys. **54** (1982) 437

4) T. Ando, J. Phys. Soc. Japan **54** (1985) 2671

5) B. Gelmont, V. Gorfinkel and S. Luryi, Appl. Phys. Lett. **68** (1996) 2171

6) T. Unuma, M. Yoshita, T. Noda, H. Sakaki and H. Akiyama, J. Appl. Phys. **93** (2003) 1586

7) H. Callebaut, S. Kumar, B. S. Williams, Q. Hu and J. L. Reno, Appl. Phys. Lett. **84** (2004) 645

8) T. Antoni, M. Carras, X. Marcadet, B. Vinter and V. Berger, Appl. Phys. Lett. **97** (2010) 042102

9) R. Nelander and A. Wacker, J. Appl. Phys. **106** (2009) 063115

10) M. Helm, in *Intersubband Transitions in Quantum wells*, edited by H. C. Liu and F. Capasso (Elsevier, 1999) 1-99

11) F. Carosella, C. Ndebeka-Bandou, R. Ferreira, E. Dupont, K. Unterrainer, G. Strasser, A. Wacker and G. Bastard, Phys. Rev. B **85** (2012) 085310

12) F. Banit, S.-C. Lee, A. Knorr and A. Wacker, Appl. Phys. Lett. **86** (2005) 041108

13) A. Wacker, M. Lindskog and D. O. and Winge, J. Sel. Topics Quantum Electron. **19** (2013) 1200611

14) H. Haug and A.-P. Jauho, *Quantum Kinetics in Transport and Optics of Semiconductors* (Springer, Berlin, 1996)

15) D. Stehr, C. Metzner, M. Helm, T. Roch and G. Strasser, Phys. Rev. Lett. **95** (2005) 257401

16) D. Stehr, M. Helm, C. Metzner and M. C. Wanke, Phys. Rev. B **74** (2006) 085311

17) A. Ghazali and J. Serre, Phys. Rev. Lett. **48** (1982) 886